POLITECNICO DI TORINO

DIMEAS - Department of Mechanical and Aerospace Engineering

Master's Degree Thesis

Miniaturization of the Rafter optical design for cubesat environment

Supervisor
Fabrizio Stesina
Co-Supervisor
Alberto Riva
Mario Gai
Deborah Busonero
Bartolomeo Montrucchio

Candidate
Fabrizio Fornasiero

Academic Year 2023/2024

Acknowledgements

A Papà e le sue corone di alloro di siepe

Abstract

RAFTER [1] (Ring Astrometric Field Telescope for Exo-planets and Relativity) is a TMA telescope concept aimed at astrometric missions, and providing a wide FOV and high optical response uniformity over an annular region around the optical axis. This thesis describes and analyzes the process of miniaturization and implementation of this idea into a Cubesat for technology demonstration purposes, and to evaluate its feasibility by analysing the performance and challenging aspects of different designs, calculating their mechanical and thermal tolerance sensitivity. We outline the critical aspects of the payload that can be tested and optimized in the framework of a dedicated CubeSat mission, in order to demonstrate the enabling technological contributors crucial to the development of a future larger scale mission. We present the results of tolerance analyses based on the inverse sensitivity of optical elements. These tolerances are then used as input for a Monte Carlo test to verify the overlapping effects given the multiple degrees of freedom. The results are presented for different sizes of the optical instrument, and a discussion on imaging capabilities for various instrument sizes is proposed. A configuration proposal is then developed: this involves mounting the optical elements into two groups. Tolerance analysis between the positions of these two groups is then conducted, and the results are compared to the scenario in which all mirrors are free to move according to all their degrees of freedom. A chapter has been dedicated to methods for analyzing stray light. An initial mechanical design has been proposed, and the incoherent irradiance has been represented on the focal plane. From this thesis, a contributing paper was written for the SPIE Astronomical Telescope + Instrumentation conference[2].

Contents

Chapter 1

Introduction

1.0.1 Exoplanets and their detection methods

The knowledge of extraterrestrial civilizations has intrigued the human mind since humanity discovered it is but a drop in the cosmic void. In this context, the search for exoplanets is considered one of the initial steps towards human resilience on an extrasolar level and is fundamental for the search for intelligent extraterrestrial life. In 1961, Frank Drake published the equation that bears his name to estimate the number of civilizations with which humanity could communicate: this estimate is the product of independent and interconnected fractions, starting from the rate of star formation to the development of extraterrestrial communication technologies. The research and characterization of exoplanets provide valuable information regarding the probability of planetary formation and insights into how this occurs, as well as enabling us to search for the fingerprints of life as we know it. The techniques used by scientists are varied; they will be briefly described, with a focus on astrometric techniques. In the search for exoplanets, particular interest lies in those located within the so-called "habitable zone" or "Goldilocks zone," which refers to the distances between the planet and its parent star where water can exist in its liquid form.

1.0.2 Techniques for exoplanet detection

There are several techniques for the search for exoplanets, including the radial velocity method, transit photometry, microlensing, timing method, direct imaging, and astrometry[3]. The latter will be discussed in a dedicated chapter.

Radial velocity Method

This method uses high-resolution spectroscopy to measure the Doppler effect on the star motion induced by the presence of an orbiting planet. The gas absorption cell technique involves overlaying the stellar spectrum with a gas of known spectrum, allowing for the calibration of the instrument's response while accounting for distortions in the spectrum. Similarly, the Thorium-Argon technique displays the spectrum of a Thorium-Argon lamp alongside the stellar spectrum for wavelength calibration. These methods reach accuracy on the order of 1 m/s.

Transit Photometry

This method uses the partial eclipse of the star by the planet to detect the variation in the star's luminosity. The probability of this phenomenon occurring is directly proportional to the radii of the star and the planet, and inversely proportional to their distance.

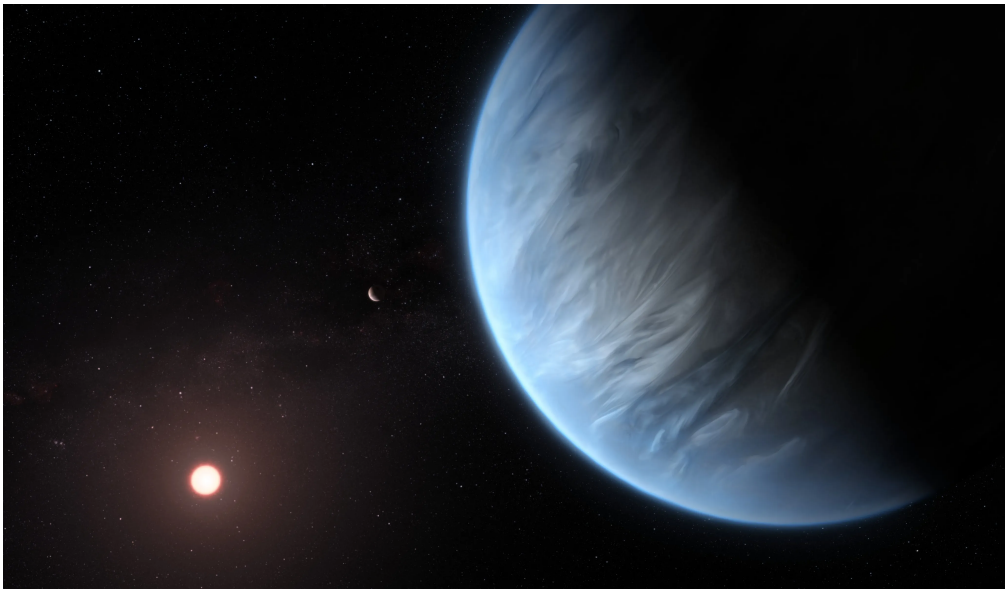

Figure 1.1: An artist's depiction of an exoplanet, credit: NASA

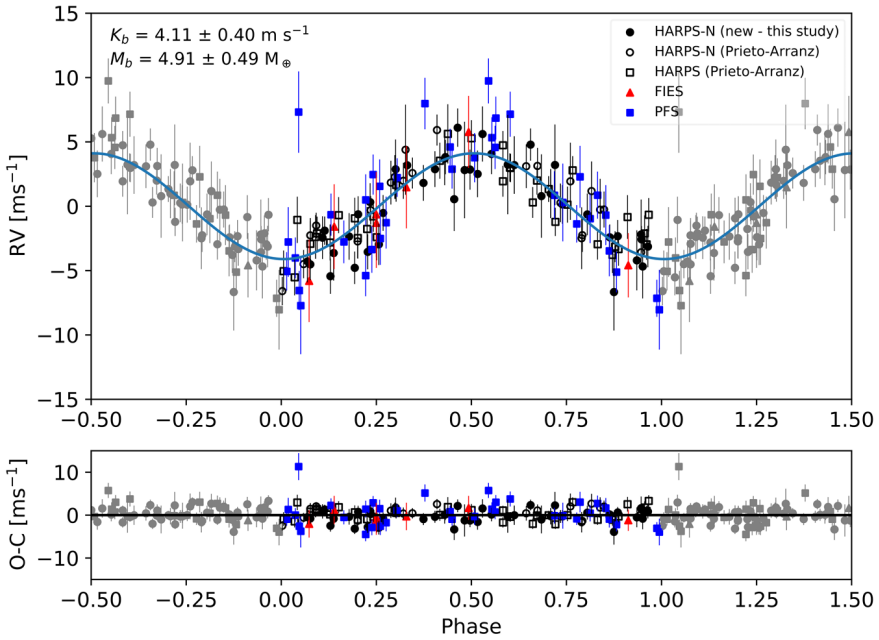

Figure 1.2: Detection of GJ 9827 b by means of the radial velocity method

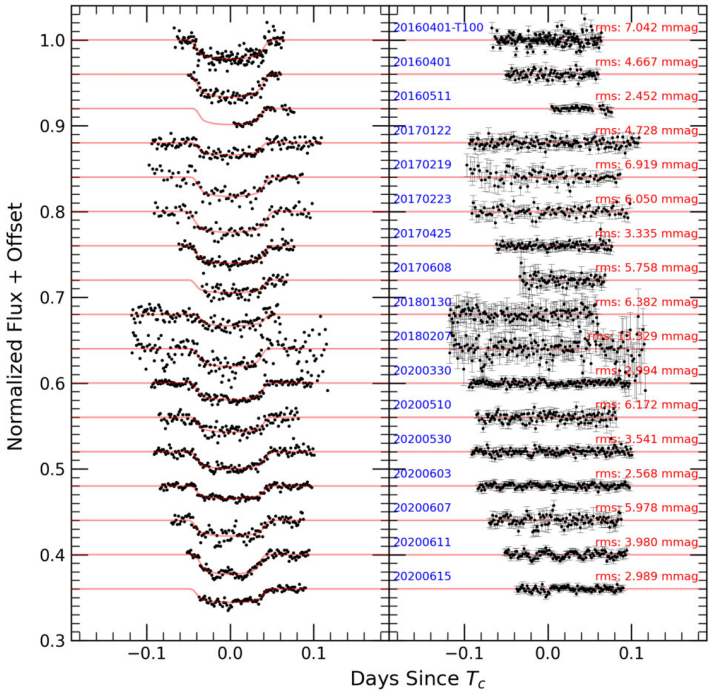

Figure 1.3: Seventeen transits of HATP-36b, the decrease in apparent luminosity is caused by the planet eclipsing its parent star[4]

Instruments for this type of detection typically have a wide field of view and are capable of monitoring a large number of stars simultaneously. Combined with spectroscopy, they allow for improved estimates from various methods and also enable the detection of the planet's spectroscopic footprints.

Microlensing

This technique uses the property of mass to bend light and act like a lens. When the star under observation moves in front of a known region, the magnification effects can be estimated, and the behavior of a single star differs from that of a planetary system. This manifests on Earth as a variation in the light coming from the star, which can be monitored. The need for a background star to be magnified makes this measurement non-repeatable.

Timing Method

In stars with periodic luminosity, such as pulsars and white dwarfs, the period is extremely stable. However, when the star is moved away or towards the observer by the presence of an orbiting planet, the time it takes for the light to reach the observer changes periodically, altering the observed period of the star. This method was used to detect the first exoplanet around a pulsar.

Direct Imaging

Direct observation of a planet is obvious at first but also highly challenging for several reasons. Firstly, the star is orders of magnitude brighter than the planet orbiting beside it, making the scattering of its light within optics as bright as, or even brighter than, the

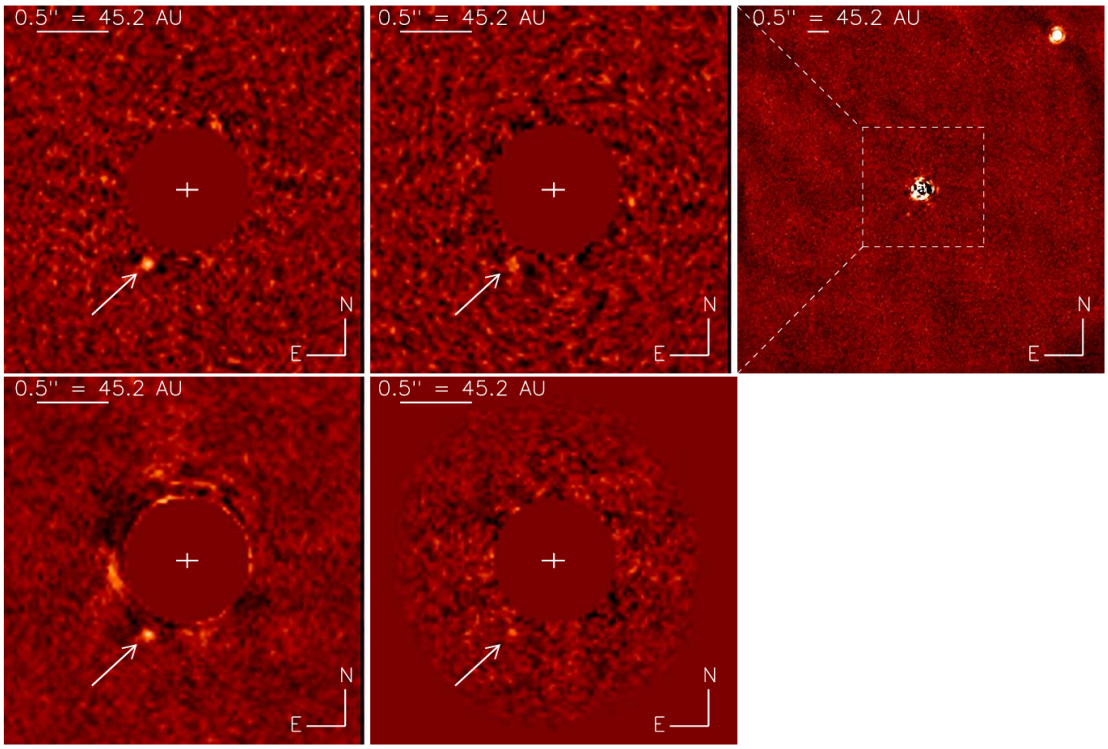

Figure 1.4: Direct observation of a probable 4-5 Jupiter-mass exoplanet to HD95086[5]

sought-after planet. Coronagraphs are thus used to mask the starlight, but often star-planet separations are too small (on the order of milli-arcseconds). Secondly, the resolution required for such observations is extremely high. Adaptive optics and interferometric techniques for starlight nulling led to the first images of planetary objects in 2005 from the ESO's Very Large Telescope (VLT).

1.0.3 Astrometry

Astrometry is a technique based on the principle that the star and the planet orbit their common center of mass. By measuring the change in position of the star, we can observe indirectly the planet's orbit. To measure its position, t is necessary to determine the center of the star's image, called the photocenter, and then understand how the actual position of the star relates to it to correct for systematic errors and distortion. The position of the star obtained in this way is then inserted into a reference system materialised by the relative positions of other nearby observed stars, called reference stars. The precision in the determination of the star position is dependent both on the optical resolution and on the brightness of the star; this dependence is explicited by the signal to noise ratio (S/N) of the observation

$$\sigma \propto \frac{\lambda}{D} \cdot \frac{1}{S/N},$$

where σ is the location uncertainty and λ is the effective wavelength. It is interesting to note that the dependence on the signal-to-noise ratio also implies a dependence on observation time. This is because a longer acquisition time results in a higher signal being captured (up to the point of pixel saturation). The maximum acquisition time is limited by the instrument's stability during data collection and the platform's pointing performance. Shorter exposures can be captured individually and then combined into a

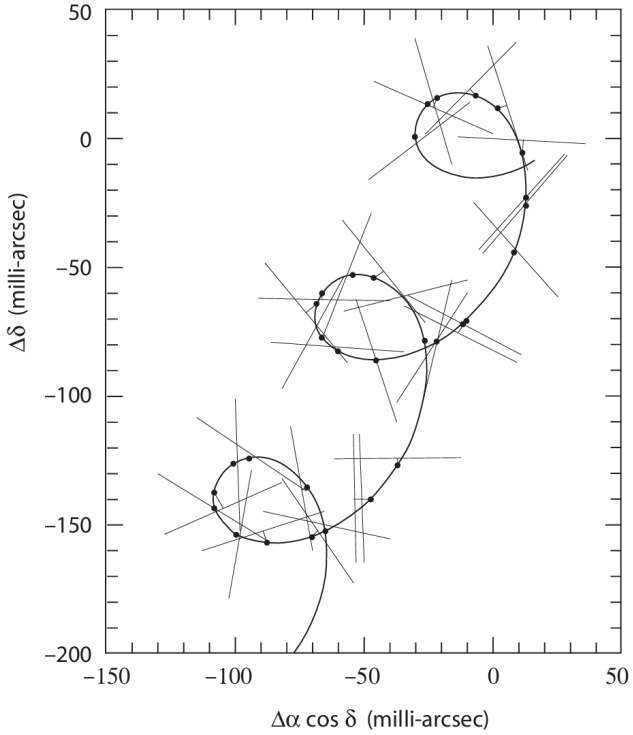

Figure 1.5: Path of a star by the Hipparcos spacecraft, Each straight line indicates the observed position of the star at a particular epoch and the curve is the interpolation of the mesurements[6]

longer acquisition to address both the detector's saturation issue and long-term pointing inaccuracies.

Point Spread Funtion (PSF)

The PSF describes the irradiance distribution from a point source. In astronomy, it is a critical characteristic of an optical system since stars are point sources with negligible angular size, in a first approximation. The final image is the convolution of the observed field with the PSF. In a perfect optical system, the PSF has a given minimum width, due to diffraction effects that limit the system's resolution, stemming from the wave nature of light. The PSF is related to the Fourier transform of the system's aperture. Non-ideal optics must consider also the geometric effects of lenses: in optical software such as Zemax, rays are approximated as they propagate through the system, adhering to the fundamental laws of reflection and refraction. The shape of the intersection between these rays and the focal plane is known as the "spot diagram," and the spot size is measured as the Root Mean Square (RMS) of the ray distribution around the chief ray. This geometric perspective is valuable for determining the optical properties and relative aberrations of a system but does not account yet for diffraction effects.

Airy Disk

The PSF from a circular aperture is known as the Airy Disk, commonly used in optical design as an initial approximation of PSF size. When the spot size is significantly smaller than the Airy Disk, the system is termed "diffraction limited," indicating that geometric aberrations are minimal compared to diffraction effects.

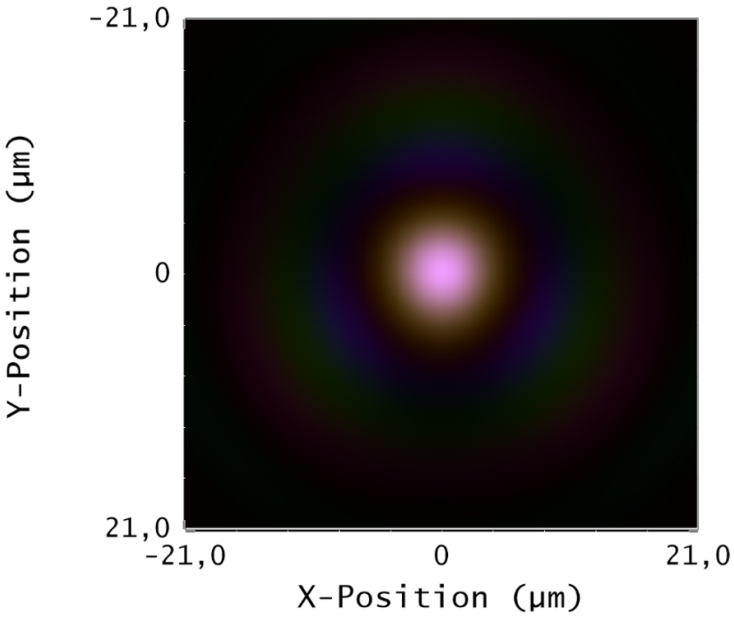

Figure 1.6: Polychromatic simulation of the Rafter Intrument's PSF, shown in true colors. Note how for longer wavelength the PSF is larger due to the effects of diffraction. The simulation is performed with the Huygens method: each ray is modelled by amplitude direction and optical path difference, their individual effect is then summed at the focal plane.

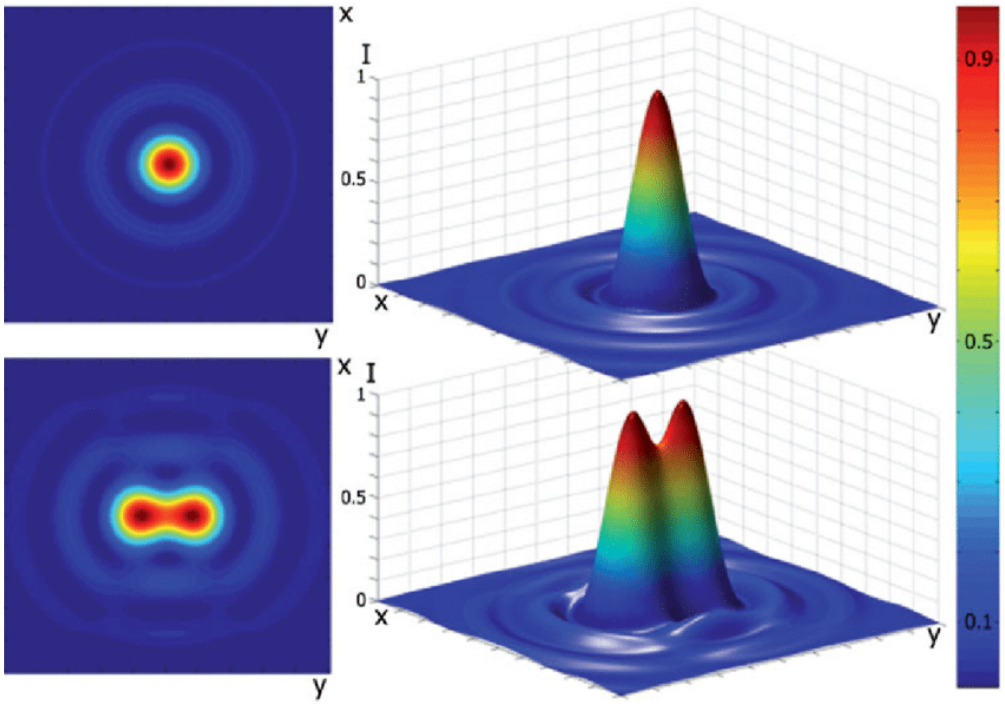

Figure 1.7: 3D rapresentation of an Airy Disk[7]. When two point sources are closer than one diameter apart their image cannot be distinguished, this is the "Rayleigh criterion"

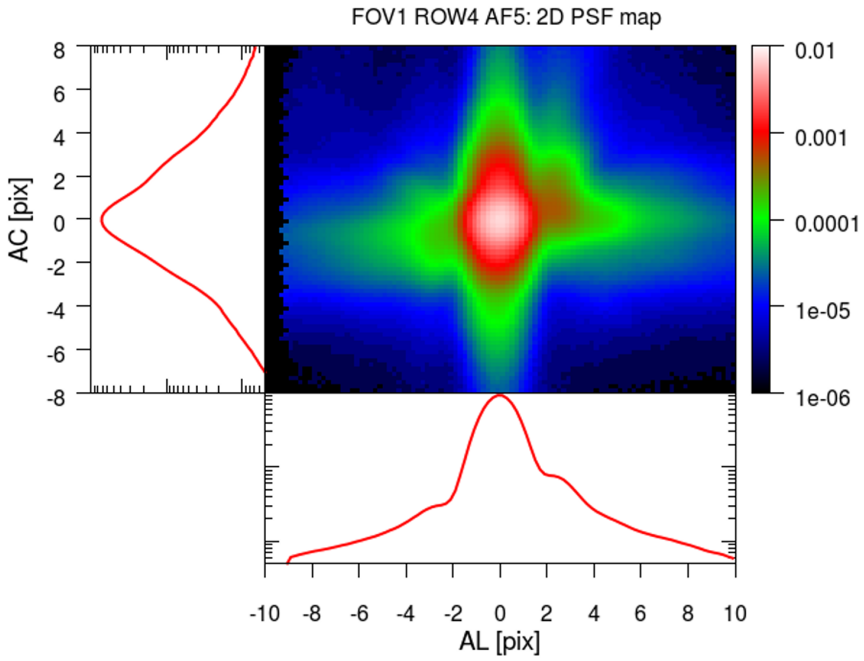

Figure 1.8: An example of a Point Spread Function in the centre of the field-of-view of GAIA. Accurate modelling is fundamental in the determination of the photocenter [9]

The size of the Airy disk also serves as a metric for resolution: when two sources are closer than the diameter of the Airy disk, they appear indistinguishable from a single source, a condition known as the Rayleigh Criterion. In terms of angular dimension, the Airy disk's size θ is inversely proportional to the diameter of the aperture D:

$$\theta \propto \frac{\lambda}{D}$$

Smaller aperture systems have lower resolution compared to larger ones due to diffraction effects.

The linear dimension d of the Airy disk on the focal plane depends on magnification M; thus, the focal length F must also be considered. The ratio $\frac{F}{D}$, known as the "f-number," is useful because it is directly proportional to the linear size of the Airy Disk.

1.0.4 PSF Calibration

The PSF is modeled across the entire field, and the center of the PSF is identified. The photocenters then undergo correction for distortions to obtain the best estimate of the angular distance among stars. In real-world scenarios, many parameters influence the shape of the point spread function (PSF), including the type of sensor, the readout method (e.g., TDI smearing), and its degradation. For polychromatic PSFs, the spectral class of the imaged star is also considered, as different spectra can shift the photocenter location. Uniformity in optical response is crucial when high precision is required[8].

1.0.5 The RAFTER mission

The mission is proposed as a compact $1m$ class instrument for the observation of exoplanets. This objective requires accuracy in the micro-arcosecond range, which in turn creates the need for strong metrological and calibration control. The RAFTER telescope is designed

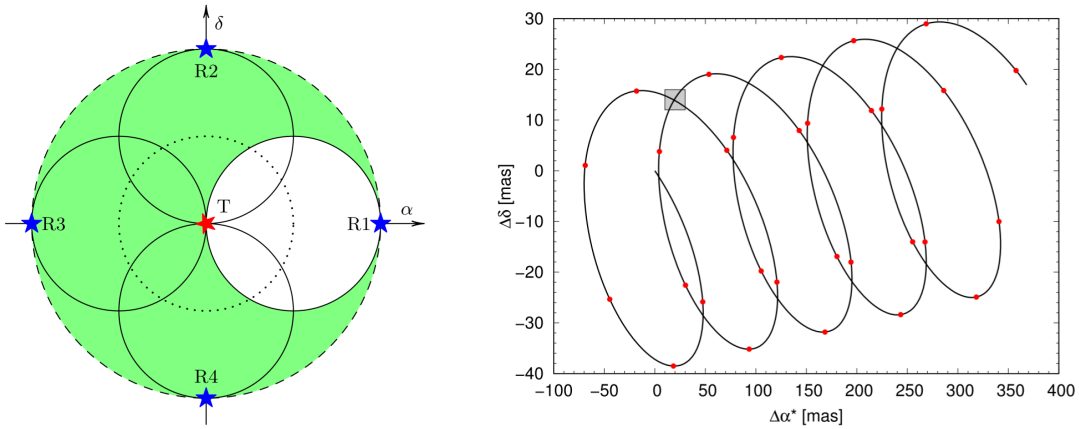

Figure 1.9:
Observational Operation Concept: The circular field of view can be utilized to access reference stars located within a 2-degree radius. By rotating the instrument, the number of observations and reference points can be increased. Thanks to measurements taken at different epochs, the stellar trajectory can be interpolated and its orbital data can be calculated.

to achieve these accuracies by combining a large field of view with uniform optical performance in the tangential direction, thanks to the circular symmetry of the optical system, and by optimizing for smooth variations in the radial direction. This reduces systematic error, simplifies alignment procedures and ensures good optical performance. The compact design allows the optical elements to be mounted in two groups of components close to each other to aid in systematic control from a mechanical point of view. The advantages (and disadvantages) from an opto-mechanical point of view are discussed in a later chapter. The large annular field with 2° diameter allows for better selection of reference star, and these ones are brighter compared tothose accessible by a rectangular FOV of the same area.[10] The mission profile, in contrast to astronomical missions such as Gaia with the objective of compiling a comprehensive catalogue of astronomical objects, has the objective of observing specific targets to significantly improve on their parameters. As shown in section 1.0.3, increasing the signal-to-noise ratio improves the precision of photometric center determination, which is crucial since global missions cannot enhance this parameter. From this point of view, it stands as a complementary mission of great scientific value in the fields of exoplanet discovery, experiments in the fields of general relativity and observation of Wide Binaries in search of MOND-like signals, and observation of microlensing from Dark Matter.

1.0.6 Rafter Instrument

The optical design of the instrument is based on a Three-Mirror Anastigmat (TMA) with a negative focal length, positioning an image plane between the secondary and tertiary mirrors. The distance between the tertiary and secondary mirrors is approximately twice that between the primary and secondary mirrors. A folding mirror is placed between the secondary and tertiary mirrors to bend the optical axis, equalizing the distances of the optical elements. This design results in a very compact arrangement divided into two groups: one comprising the secondary and tertiary mirrors, and the other including the primary mirror, the folding mirror, and the focal plane. The focal plane is arranged

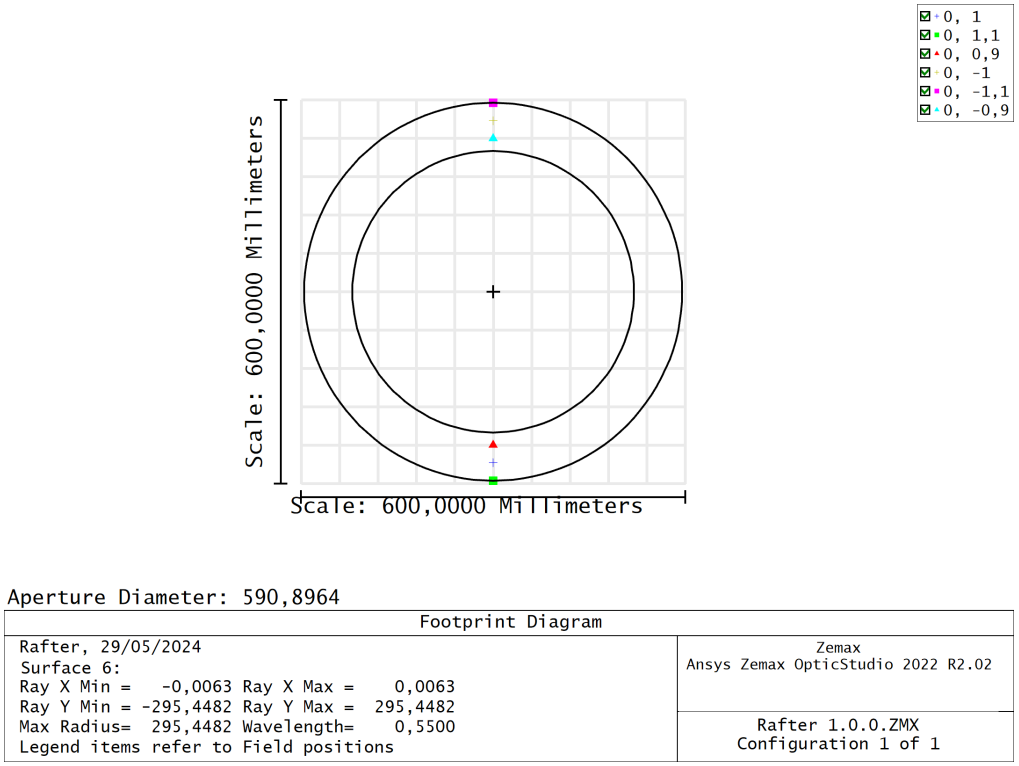

Figure 1.10: Focal plane layout, FOV is 2° degrees in diameter and 0.2° in the radial dimension. The positions shown are the same used in the tolerancing process for spot size evaluation and are weighted equally.

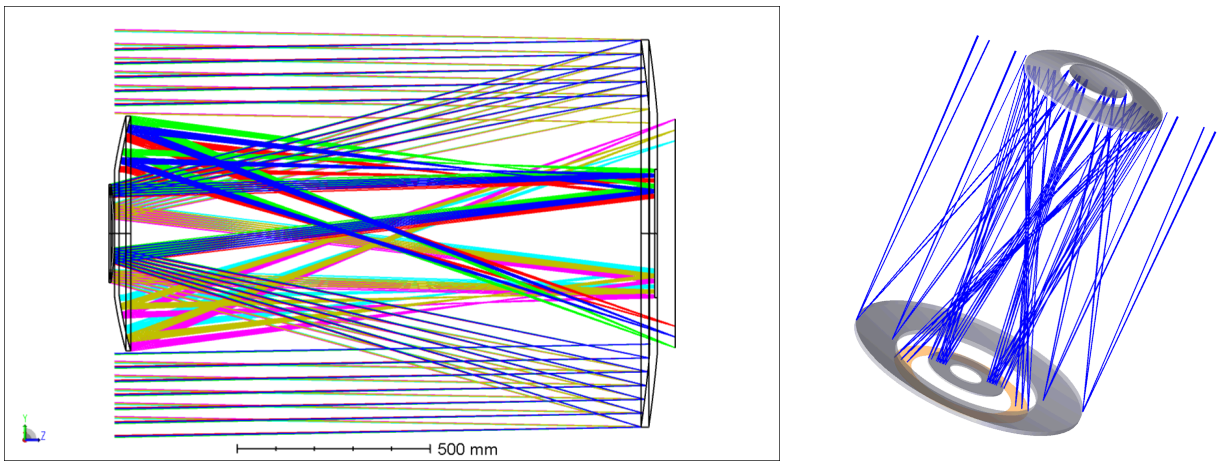

Figure 1.11: Rafter instrument optical diagram and 3D representation

around the folding mirror and is surrounded by the primary mirror. The instrument has an overall focal length of 15 meters and a primary mirror of approximately one meter in size, resulting in an instrument length of 1.4 meters. The field of view has a 2-degree diameter and a width of 0.2 degrees.

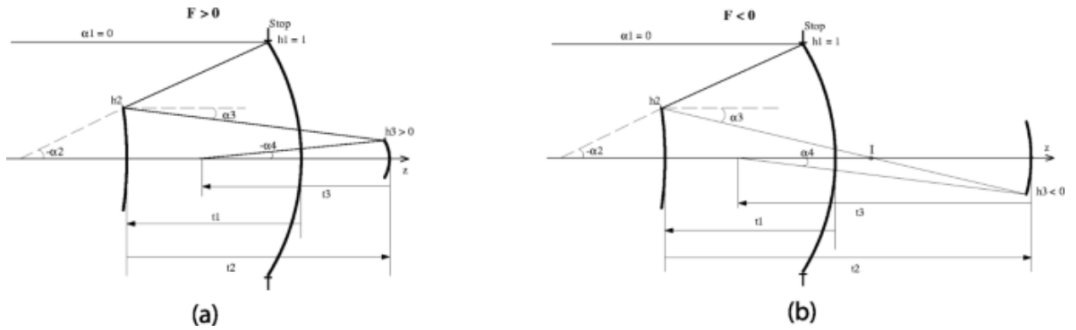

Figure 1.12: Two types of Three Mirror Anastigmat designs, on the left a positive focal length design, on the right a negative one. Note how, in the second design the distance between the secondary mirror and the tertiary is almost double the primary-secondary distance [11]

Performance

The six chosen fields for analysis are: the center of the field, the outermost edge of the field, the innermost edge, and these three points reflected across the optical axis.

As expected from the original Korch design of 1972, all third-order aberrations are well controlled, with the first and second mirrors compensating each other for coma and spherical aberrations, and the third mirror reducing the Petzval sum and astigmatism. Distortion is present but can be disregarded as it is accounted for during the calibration stage.

The most prominent high-order aberration present is some trefoil, as evidenced by the shape of the Point Spread Function (PSF).

Geometric ray tracing places all rays within the Airy disk, with a Strehl ratio of 0.982; thus, geometric errors are negligible compared to diffraction effects.

Therefore, the Rafter instrument meets the mission's requirements.

1.0.7 Concept Demonstration

The concept presented is at a Technology Readiness Level (TRL) of around 2. Previous studies have demonstrated the feasibility of the scientific concept, and optical design proposals meeting the requirements have been formulated. The next stage, TRL 3, involves experimental testing and practical demonstration of the concept. This milestone aligns with the practical nature of the project's benefits, which lead to an operational advantage that is difficult to quantify otherwise. A concept demonstration is therefore a logical next step in the project's progression.

The use of small satellites and smaller platforms like CubeSats is common in the space industry, leveraging their modularity and low launch costs to test new platforms and technologies for operational response in the low Earth orbit space environment. In addition to cost advantages, these platforms often benefit from less restrictive regulatory considerations, as missions are often considered disposable. These factors contribute to rapid development compared to larger missions and allow for iteration of multiple CubeSat missions before finalizing the design.

Miniaturization of the concept must be part of a thorough study. This work has investigated optomechanical tolerances, emphasizing trend over a detailed analysis. However, the future work chapter is focused on the further analysis that could lead to the

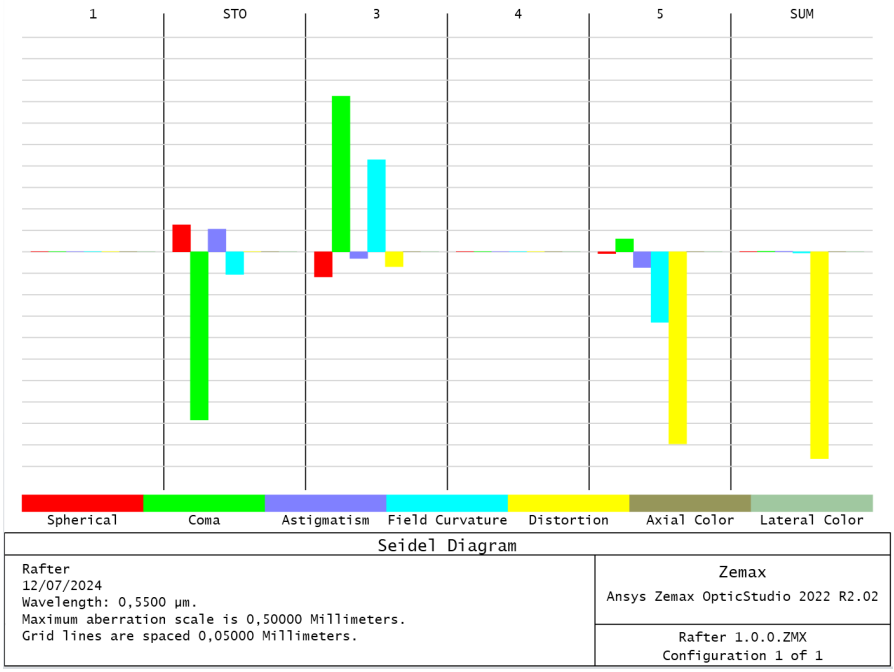

Figure 1.13: Seidel Coefficients for the different optical elements of the instrument are provided, noting that element number 4 has no optical power since the folding mirror only bends the optical axis. The total on the left shows the sum of all contributions: these coefficients represent the wavefront error at the pupil of the overall optical system.

development of an effective scientific demonstrator representing the final instrument.

Initially, the optical design remains unchanged from that of the full mission. Modifications must be justified by practical necessity and will not be studied in this work. One of the initial questions to address is whether the miniaturized demonstrator is representative of the concept. Manufacturing capabilities for small mirrors differ from those for meter-scale components. Similarly, a tolerance of 1 mm in a 1 m system translates to a tolerance of 0.1 mm in a 10 cm system. Understanding which variables scale with size and their relationship to the demonstration is crucial.

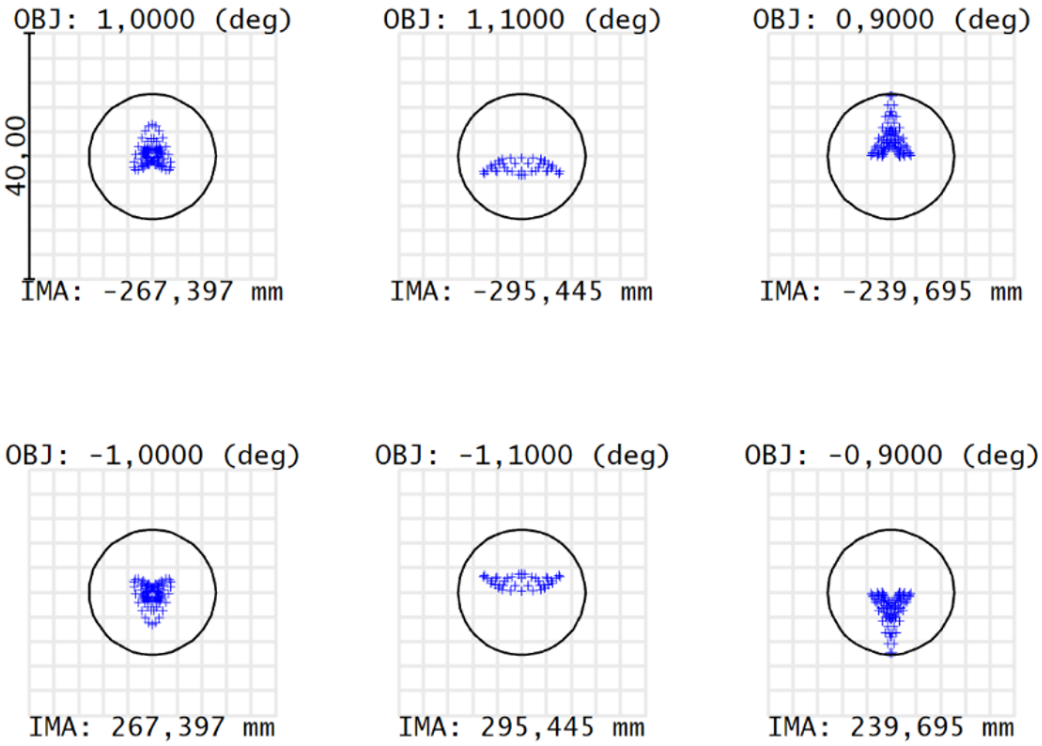

Figure 1.14: Spot distribution plot for points on the focal plane: these plots represent the intersection of the geometric rays with the focal plane. The diagrams on the left are for the center of the field, the two central ones are at the inner edge of the field, and on the right is the outer edge. The Airy disk, shown in black, represents the size of the PSF due to diffraction.

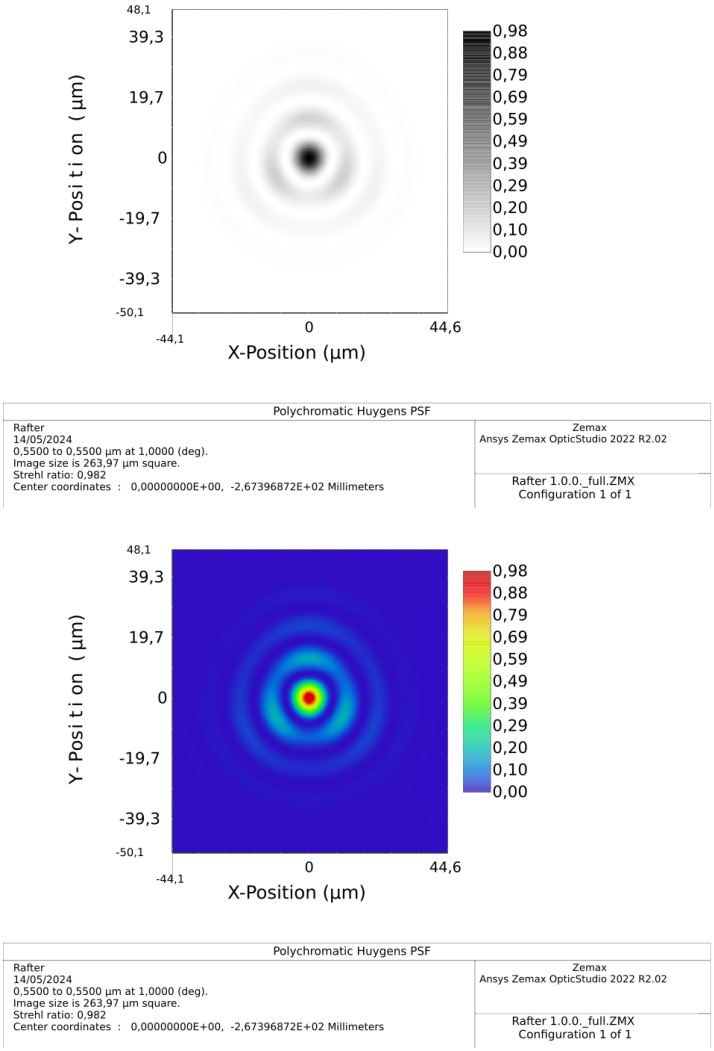

Figure 1.15: Monochromatic simulation of the PSF of RAFTER in the central field, shown on the left in linear scale and on the right in false color on a logarithmic scale.

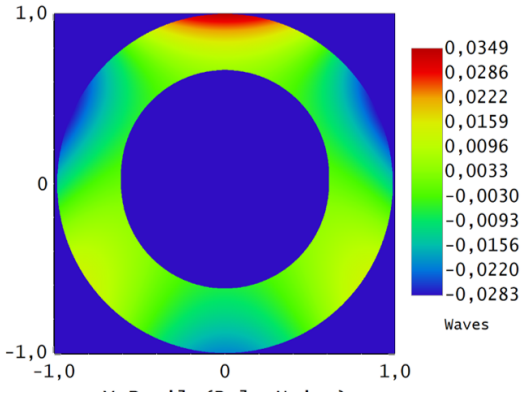

Figure 1.16: Wavefront Error in the pupil for the center field. Higher order trefoil aberration and very low amount of residual astigmatism is present. Due to the localized wavefront error, vignetting factors can be introduced to mechanically obscure part of the pupil for better geometrical correction at the cost of light

Chapter 2

Miniaturization and the effect on instrument performance

Miniaturization, the process of scaling down the size of systems and components, poses significant challenges, particularly in the field of optical systems. This thesis discusses the mechanical implications of miniaturization on optical instruments, highlighting the complexities and considerations involved. When an optical instrument is simply scaled down, the mechanical properties do not scale proportionally. The tolerances, which are the permissible limits of variation in a physical dimension, are affected by the scale factor. This non-linear scaling of tolerances can lead to manufacturing complications or downright impossibility in building by the available technologies. Metrological control, the science of measurement, becomes increasingly difficult as the size of the optical system decreases. For instance, active control systems in telescopes, which adjust the optical elements to maintain alignment, become problematic when miniaturized. The metrological system may become disproportionately heavy compared to the rest of the optical components, making direct scaling impractical. The production techniques for optical components such as mirrors also change with scale. Fabricating a large mirror, for instance, is often more straightforward than producing a smaller one with the same precision. This is due to the differences in manufacturing technologies required for different scales. Techniques suitable for large-scale production may not be applicable or efficient for smaller scales. The design of the mechanical support for optical components must also be reconsidered during miniaturization. A support system for a large mirror may not be suitable for a smaller mirror, requiring a completely different approach to ensure stability and performance. This means that an optical design cannot be simply scaled down without a comprehensive redesign of its mechanical structure. When selecting the scale factor for an optical system design, it is essential to ensure the scale accurately represents mechanical challenges and objectives, is manufacturable, and meets mission-specific performance requirements. Miniaturization reduces resolution and light capture, necessitating a careful evaluation of acceptable performance degradation.

2.1 Diffraction Limited Resolution

The scaling of the dimension of the aperture has an obvious impact on diffraction performance, this is commonly evaluated using the Rayleigh criterion defined as:

$$\theta \approx 1.22 \cdot \frac{\lambda}{D}, \tag{2.1}$$

where λ is the center wavelength and D the diameter of the circular aperture. However, given that the telescope as shown has an obscuration ratio of $\approx 61\%$, the real PSF must be taken into account when defining the angular resolution.

Other aspects of scaling this optical instrument is light gathering capabilities, in this regard, it's expected to decrease as the area (D^2).

2.2 Photometry Analisys

To give a qualitative idea of the brightness of the object that can be imaged, a fixed exposure time and spectral characteristics are hypothesized, one minute and a black body of $5500K$ respectively and a plot of magnitude is presented to obtain a specific S/N. The simulation assumes a star as a black body of given temperature and the irradiance is computed by integrating the spectrum over the visible range. The power is then projected at the aperture of the system, converted into photons, and arrives in an area of the size of the Airy disk. The CCD equation in computed and then the script is solved backwards to obtain the magnitude capable of giving a given S/N ratio. The angular resolution in arcseconds is also computed for the diameter.

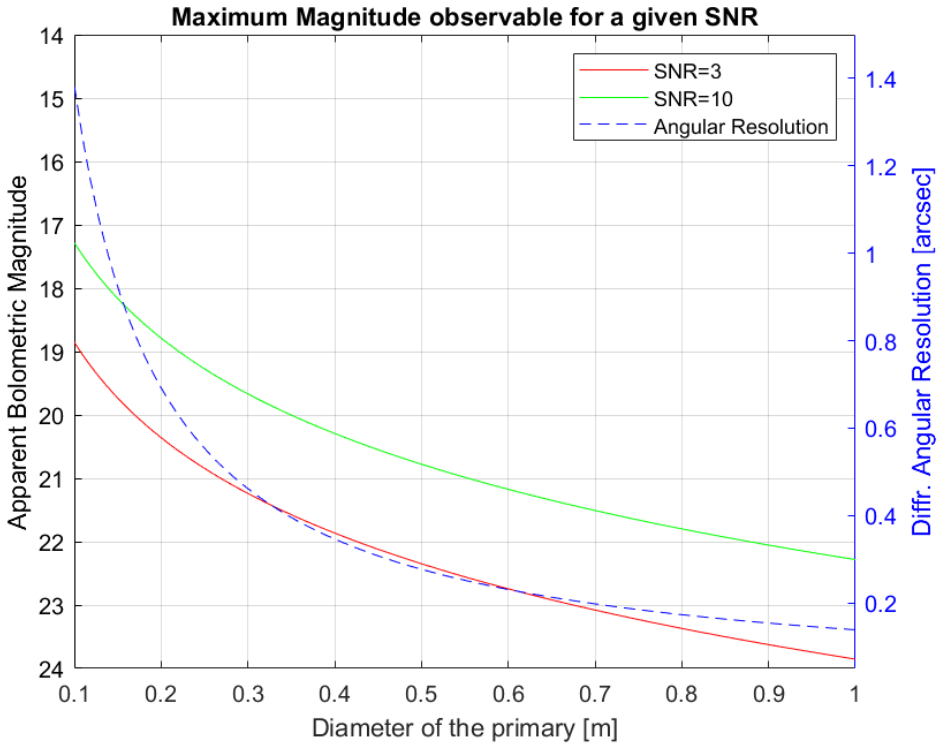

Figure 2.1: Simulation of the maximum magnitude of a G star capable of producing a given S/N ration on a pixel of the detector. The parameters are: $exposure\ time = 60s$, $black\ body\ temperature = 5500K$, $quantum\ efficiency = 75\%$, $dark\ current = 3e^{\smile}/p/s$, $readout\ noise = 3e-$, $pixel\ size = 4 * 10^{-}6$, the reason for the specified pixel size is because the Airy disk size for the f-number is computed and the energy is distributed over that area of pixels.

The graph in Fig 2.1 serves as a general guideline, with its parameters chosen arbitrarily yet sensibly based on the current technology on the market. Each parameter in the

simulation requires a trade-off and careful selection based on available components, cost and specification. The graph primarily provides an indicative understanding of the potential performance of a system of that scale.

Chapter 3

Tolerancing for miniaturization

3.0.1 Introduction

The process of tolerance analysis is non-deterministic and lacks a defined workflow; tolerancing must accurately represent the optical instrument assembly configuration and consider both manufacturing technology and cost associated with tighter tolerances within the project context. This process is inherently iterative, increasing in detail over time. Starting from optical requirements and defining a performance metric, the range of allowable optical element positions can be determined to achieve an acceptable level of performance. The relationships between degrees of freedom and mechanical mounting must be considered, introducing constraints that constantly need to be evaluated against available production technologies and project budget.

Zemax Optics Studio R2022 [1] provides several tools internally for tolerance analysis, both in sequential and non-sequential modes. They can be categorized as follows, noting that the first two operate on one dimension at a time, while Monte Carlo considers compound effects:

- Sensitivity: Each degree of freedom of the design is perturbed by the same amount, and the resulting change in a (user-defined) performance parameter is monitored, and presented to the user in tabular form. This tool is used to identify which degree of freedom is most sensitive to perturbation, establishing a hierarchy useful for initiating mechanical design and understanding which degrees of freedom require metrological control.

- Inverse Sensitivity: Similar to Sensitivity, but operates in reverse. Given a performance limit, the program iteratively adjusts individual optical elements while monitoring the performance parameter until the set value is reached. The adjustments are then reported to the user.

- Montecarlo: While the previous analyses focus on one degree of freedom at a time, the Monte Carlo approach assigns a statistical distribution to each degree of freedom. In each iteration, every degree of freedom is randomly varied according to its statistical distribution, and the performance of the perturbed system is saved. After running enough iterations, the statistical analysis can determine the expected performance of a real system where each degree of freedom deviates independently from ideal conditions.

[1] The educational licence was provided by Politecnico di Torino

3.0.2 Method

To quantify the impact of miniaturization on the mechanical tolerance of optical elements, a tolerance analysis was performed. This analysis involved an inverse sensitivity calculation to determine the permissible displacement of an element in one of the selected degrees of freedom to a specified limit. Specifically, the system was allowed to deteriorate until the root mean square (RMS) spot size doubled the diameter of the Airy disk, whose nominal value is 10 μm. Following the inverse sensitivity analysis, the "high precision" preset tolerances from Zemax OpticStudio was used as a baseline, and the tolerance data was updated with the most stringent values. A Monte Carlo simulation, consisting of 1000 iterations, was then conducted to assess the effect of simultaneous movements in all degrees of freedom, comparing the individual tolerance effects to the collective impact of all optical elements moving concurrently. The resulting spot size distribution was then plotted in Figure 3.3.

In the subsequent section, various cases are compared to evaluate the effects of scaling the optical system and of mounting the optical elements in two separate groups. From a scientific point of view, a better indicator of astrometric performance should be chosen, the Airy disk is indicative of the size of the PSF, which is one of the benchmarks, limiting factors of position determination are systematic errors in optical alignment and calibration: effects of de-skewing on disorientation should also be taken into account

3.0.3 Scaling of the instrument

Analysing the scale of the instrument and its changes is the starting point for defining a meaningful technical demonstrator. Ideally one would want to demonstrate the capabilities of the instrument by building it at full scale, but this would be impractical because it would lead to exceedingly high costs. However, in reducing the scale, there is a risk that the tolerances will not be comparable to the real instrument and the demonstration will not be meaningful. Clearly, the concept can (and should) be verified with a scale-optimised design according to the most convenient manufacturing technologies in terms of price and performance. In this study, it was decided to keep the design constant in order to study only the size effect.

With this in mind, it was studied how changing the scale, quantified by the diameter of the primary (1 m in the nominal case) changes the sensitivity to mirror movement to a fixed performance indicator, in this case, the Root Mean Square of the spot size.

Different scales of the optical configuration have been subject of study. The nominal $1\,m$ primary diameter has been scaled down, the two smaller sizes of $0,2\,m$ and $0,1\,m$ are of particular interest for cubesat application as they constitute an instrument of 2U and 1U in diameter respectively.

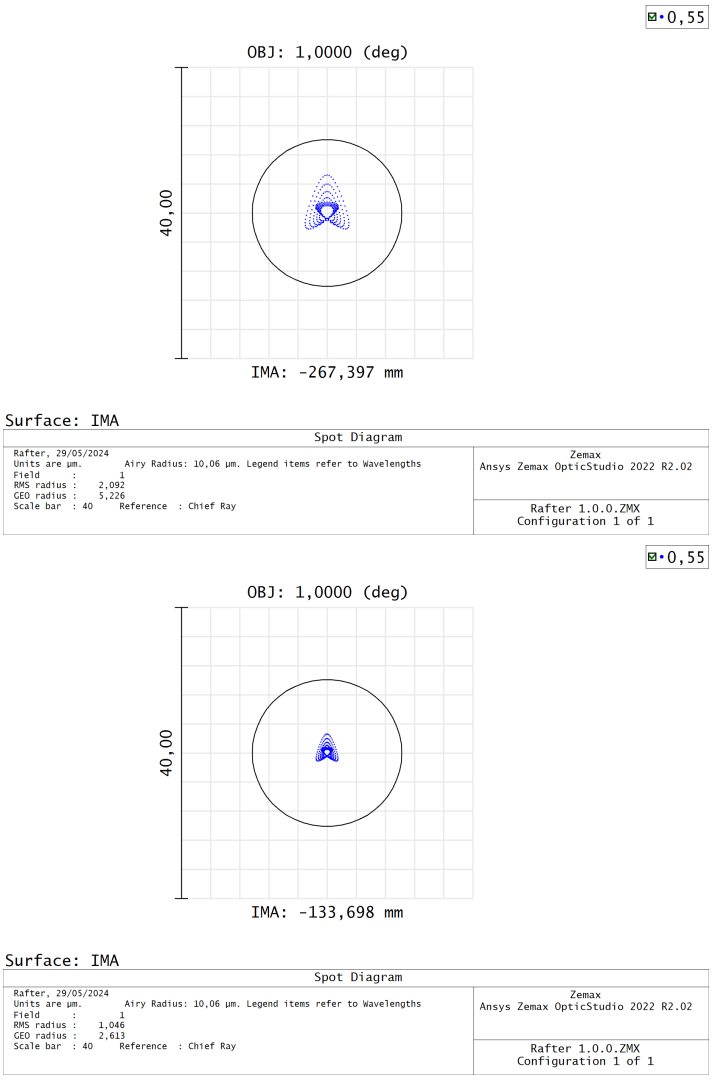

Figure 3.1: The figure shows the spot sizes at the centre of the annular field (1 deg from the optical axis) for the 1m primary case (above) and the 0.5m case (below). Note how the spot size from the geometric ray trace scales exactly with the rest of the instrument while the airy disc, a function only of the dimensionless aperture and wavelength, remains unchanged in linear size. This diffractive effect allows for greater mechanical tolerance in the system.

Table 3.1: All of the distances are in mm and angles in deg unless stated otherwise. The fringes units are relative to a wavelength of 633 nm.

Degree Of Freedom	**1.0 scale**	**0.5 scale**	**0.25 scale**	**0.2 scale**	**0.1 scale**
Primary Mirror curvature (1/[mm])	$\pm 0,023$	$\pm 0,023$	$\pm 0,023$	$\pm 0,023$	$\pm 0,023$
Secondary Mirror curvature (1/[mm])	$\pm 0,034$	$\pm 0,035$	$\pm 0,036$	$\pm 0,035$	$\pm 0,035$
Folding Mirror curvature (fringes)	± 1	± 1	± 1	± 1	± 1
Tertiary Mirror curvature (1/[mm])	$\pm 0,200$	$\pm 0,200$	$\pm 0,200$	$\pm 0,200$	$\pm 0,200$
Primary - Secondary distance	$\pm 0,011$	$\pm 0,011$	$\pm 0,011$	$\pm 0,011$	$\pm 0,011$
Secondary - Folding distance	$\pm 0,158$	$\pm 0,159$	$\pm 0,159$	$\pm 0,159$	$\pm 0,161$
Folding - Tertiary distance	$\pm 0,200$	$\pm 0,200$	$\pm 0,200$	$\pm 0,200$	$\pm 0,200$
Primary Decenter	$\pm 0,138$	$\pm 0,139$	$\pm 0,141$	$\pm 0,139$	$\pm 0,142$
Primary Tilt	$\pm 4,415E-3$	$\pm 8,879E-03$	$\pm 0,018$	$\pm 0,022$	$\pm 0,045$
Secondary Decenter	$\pm 0,139$	$\pm 0,140$	$\pm 0,143$	$\pm 0,140$	$\pm 0,143$
Secondary Tilt	$\pm 0,014$	$\pm 0,027$	$\pm 0,066$	$\pm 0,068$	$\pm 0,164$
Folding Decenter	$\pm 0,200$	$\pm 0,200$	$\pm 0,200$	$\pm 0,200$	$\pm 0,200$
Folding Tilt	$\pm 0,024$	$\pm 0,048$	$\pm 0,159$	$\pm 0,121$	$\pm 0,200$
Tertiary Decenter	$\pm 0,200$	$\pm 0,200$	$\pm 0,200$	$\pm 0,200$	$\pm 0,200$
Tertiary Tilt	$\pm 0,082$	$\pm 0,164$	$\pm 0,200$	$\pm 0,200$	$\pm 0,200$
Surface Irregularity for all surfaces	$\pm 0,2$	$\pm 0,2$	$\pm 0,2$	$\pm 0,2$	$\pm 0,2$

It is interesting to note that many linear displacement tolerances do not seem to change significantly, however, the angle tolerances show an inverse linear trend with respect to the scaling factor: this can be interpreted as the same linear deviation, as when the length is halved, the angle approximately doubles (assuming small angles). As shown in the Figure3.1, the geometric spot size decreases with the scaling factor, while the Airy disk, representing the diffraction limit, remains unchanged. This allows for greater geometric degradation. This result does not necessarily imply a better manufacturability of the instrument since the variation of the size of the mirrors and the smaller radii of curvature lead to other complications, a more in-depth study should also take into account the construction requirements when determining the size of the instrument: this thesis focuses on the optical result of these variations.

3.0.4 Mounting in groups

One of the main advantages of the RAFTER design is its compact layout on the optical axis, which allows all elements to be mounted in two groups: the front one, on which the secondary and tertiary mirrors reside, and the rear one, on which the primary, folding mirror and focal plane are located, as shown in 3.2. The possibility of reducing the degrees of freedom is advantageous from an operational point of view, since the assemblies can be integrated on the ground with a higher degree of precision and then aligned with each other, either in the process of payload integration or by active adjustment in orbit. It is therefore of interest to study the tolerances between the two: to a first approximation, therefore, the assemblies are considered perfectly assembled and the only dimensions that can change are those of their mutual relationships (angle and separation). The 1 metre diameter of the primary has been fixed and the process of defining the tolerances is the same as in the previous chapter, the inverse sensitivity has been calculated with a limit equal to an RMS spot size equal to twice the Airy disc and a simulation is then performed to evaluate the compound effect: limiting the degrees of freedom proves advantageous from this point of view. The histogram in Figure 3.3 represents the distribution of the RMS of the geometric spot size of the Montecarlo of the two configurations and highlights how fewer degrees of freedom decreases the compounding effect of the errors, obtaining a statistically better performance by approximately a factor 2.

Table 3.2: Comparison of inverse sensitivity results between the movement of the primary mirror and the movement of the two assemblies.

DoF	**Only Primary Mirror Movement**	**Movement of the two groups**
Distance	$\pm 0,011$	$\pm 0,010$
Tilt	$\pm 4,415E-03$	$\pm 0,012$
Decentering	$\pm 0,138$	$\pm 0,137$

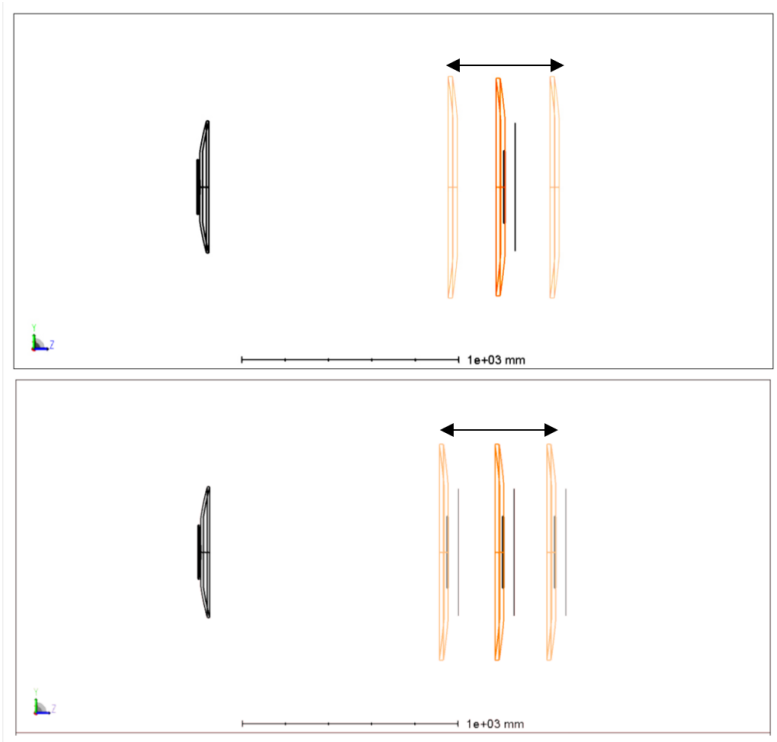

Figure 3.2: The diagram shows the movement of the primary mirror in the two configurations, at the top, the free movement of the element, at the bottom, the constrained system assuming it is mounted in two assemblies.

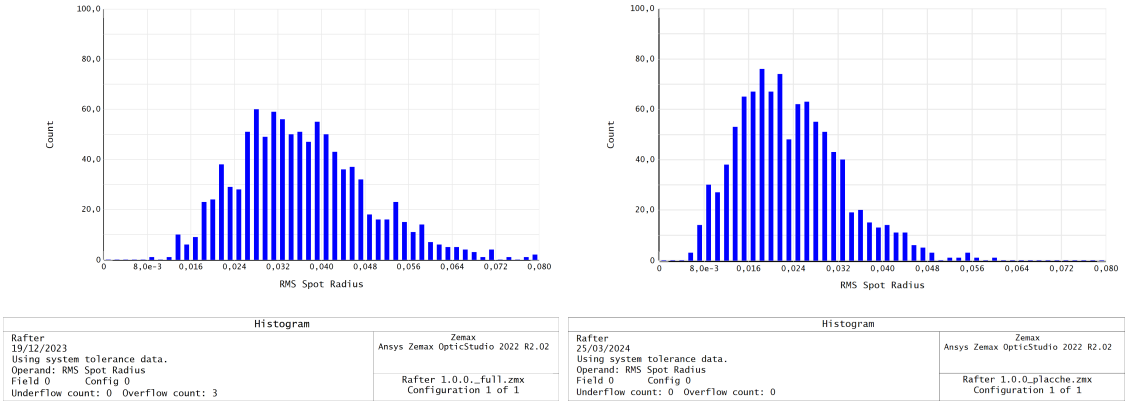

Figure 3.3:
Distribution of spot size in the Monte Carlo simulation: the tolerances, calculated individually with inverse sensitivity and a spot size limit equal to twice the Airy disk, overlap. On the right is the case where all mirrors can move, while on the left is the case where the groups are aligned and have the freedom to move relative to each other.

Chapter 4

Stray Light

The study of stray light is a nonlinear process aimed at minimizing the amount of unfocused light that reaches the sensor or sensitive elements of the instrument. Zemax offers a calculation mode called "non-sequential" that models the mechanical configuration of the system. Instead of sequentially tracing rays through the optical elements, this mode separates rays at each interaction with an element into refracted, reflected, and scattered components, which are then propagated further through the system. This approach allows for a more accurate simulation of light behavior while simulating only a single geometric ray. Rays with low intensity, below a predefined threshold, are neglected to conserve memory. Scattering and reflection are also numerically modeled, and only a handful of rays are propagated for each ray parent when scattering occurs. The starting point is the optical system enclosed in a cylinder with 95% absorption material, which also fills the spaces between mirrors. One method to evaluate the light response is to calculate the Point Source Transmittance (PST). The methodology is as follows: a point source with known emissivity is placed on-axis, and its irradiance on the focal plane is measured. The source is then moved away from the image center up to a known limit. The PST plot displays the irradiance reaching the focal plane for each source position. This plot identifies the light arrival angles that have the greatest impact on the focal plane. When the light source is within the field, this effect is considered in the sequential optical analysis. However, when the source exits the field, this light is considered stray. Stray light usually is either reflected from inside the instrument (e.g., illuminated mechanical elements) or scattered from one of the illuminated surfaces. The polarization of scattered

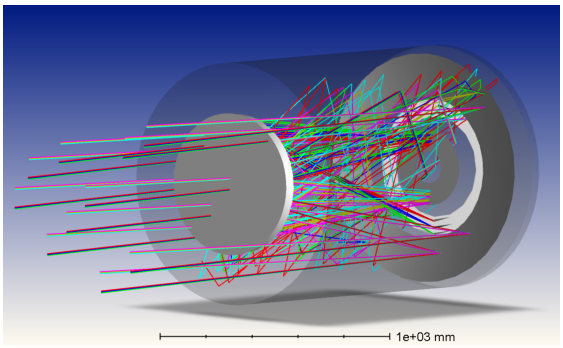

Figure 4.1: Non Sequential ray trace simulation: The rays originate from collimated material sources inserted into the code at various points in the field. These rays can either reflect geometrically or generate additional rays through Lambertian scattering. The diagram shows only a few of these rays, and their intensity is not uniform.

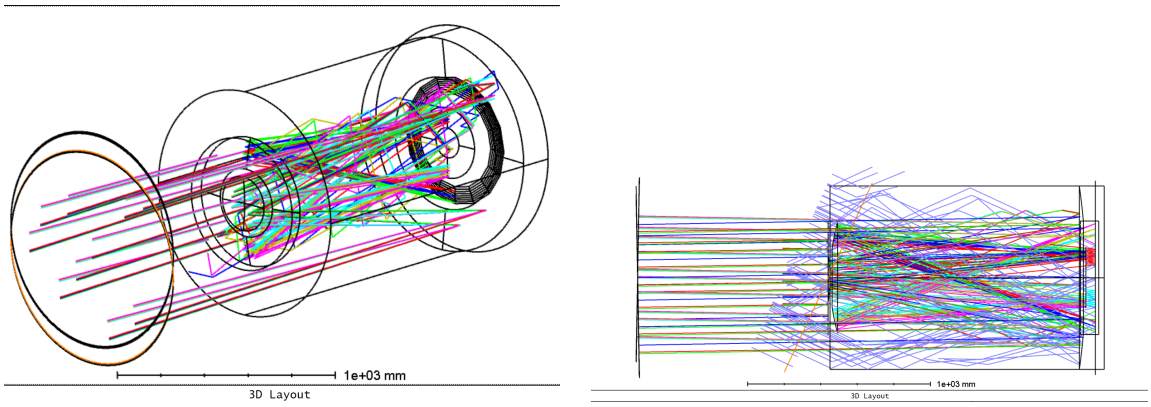

Figure 4.2: Representation of the non-sequential raytrace: a source is placed at a chosen angle, in this case, 7.5° from the optical axis. Many of these rays reflect off the surface of the optical tube in which they are mounted and can reflect off all surfaces they encounter. These rays are purely geometric and are assigned an irradiance value. During the simulation, $1 * 10^6$ rays are simulated and, if they reach it, are recorded at the focal plane. This non-collimated light reduces the signal-to-noise ratio and needs to be mitigated.

light when it strikes a partially reflective surface is simulated as perfectly Lambertian. A subsequent phase of this analysis involves identifying critical surfaces that, if illuminated, are in the line of sight of the focal plane and can reflect onto it. After determining the PST, if unacceptable results are found at certain angles, a non-sequential ray trace is performed in that configuration. Non-sequential ray tracing involves the propagation of rays from light sources set in the program, with each source emitting a million rays. These rays propagate through the system, reflecting and scattering according to user-defined limits, generating a database of parent and child rays. Each ray, upon reflection, produces additional rays due to scattering. This calculation generates a database of rays that can be filtered, one of which identifies the intersection point with the focal plane. Critical surfaces and the path rays take to reach the focal plane are then identified. A mitigation plan is proposed, which may include baffles and light traps. The process iterates until results are acceptable across all specified conditions.

4.0.1 PST Analisis

The mechanical system of Rafter was modeled starting from the optical design, with additional mechanical elements incorporated. Specifically, the system was housed within an optical tube, and non-reflective material was inserted between the mirrors, while the focal plane was integrated with the rest of the system. All mechanical elements were conservatively modeled with a 95% absorbing material that produces Lambertian scattering. Higher absorption values are readily available in commercial paints, but this analysis aims to determine critical paths and identify routes where light can reach the focal plane with minimal reflections.

The focal plane was modeled as an annulus, divided into virtual pixels. Collimated sources were then placed within the field of view, and their projection onto the focal plane was verified. Similarly, a total irradiance source of 1 W was positioned to fully illuminate the entrance pupil. A merit function was constructed within Zemax using the total irradiance on the focal plane, allowing evaluation of how much energy reaches the focal plane.

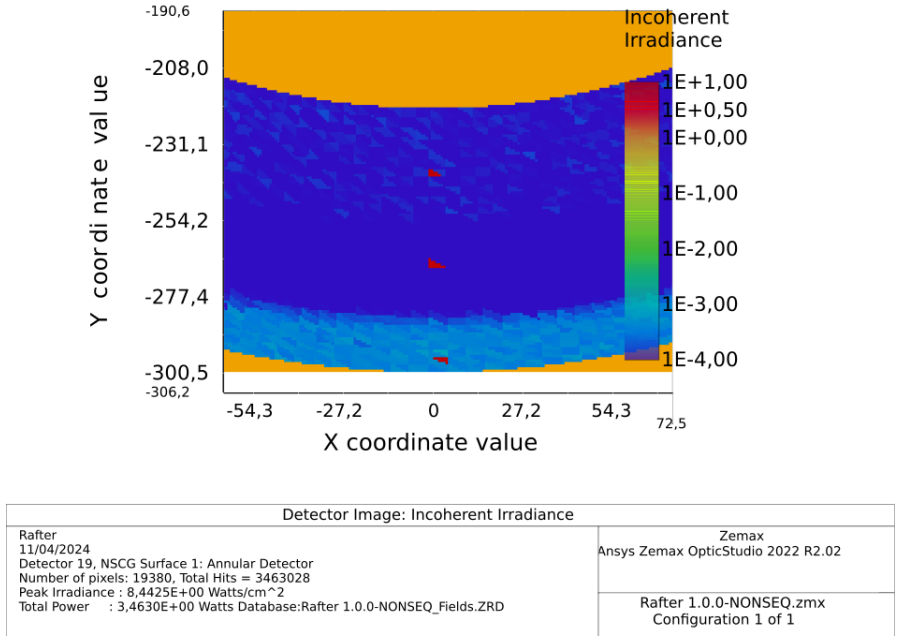

Figure 4.3: Result of the non-sequential simulation where the sources are within the field (the same ones represented in the spot diagram). For numerical reasons, the focal plane is divided into cells, and it can be observed that almost all the light falls collimated on the sensor, generating the image. However, some of the light disperses and hits the outer edges of the field in a non-collimated manner.

This test source was rotated around the entrance pupil until it exited the field of view: all light hitting the sensor from this angle onwards is considered stray light. The process can be automated using a script to construct the PST. It can be observed that at 7.5°, the maximum intensity occurs. In this scenario, the focal plane can be examined to observe how energy is distributed.

In subsequent work, based on these data, the primary reflection paths can be analyzed, and a mitigation strategy can be proposed.

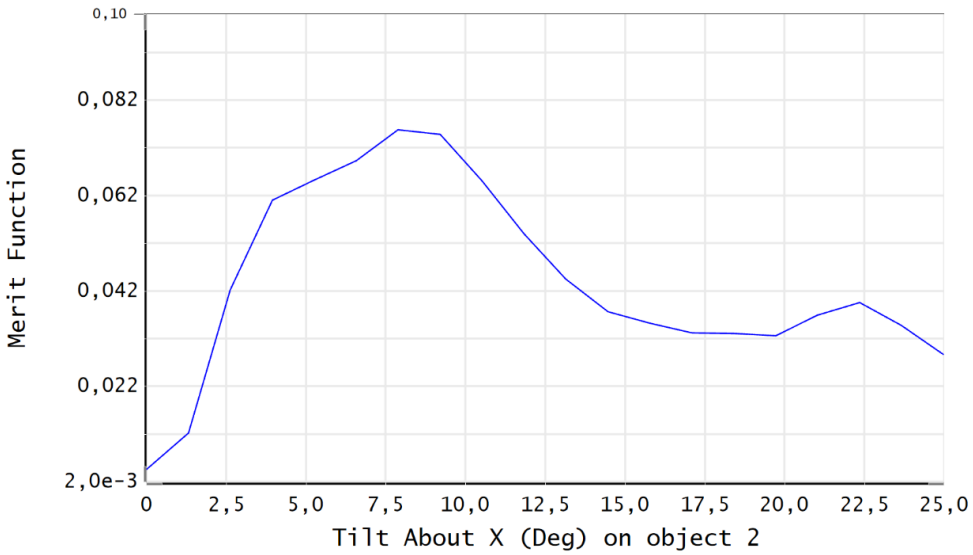

Figure 4.4: PST of the configuration in Figure 4.2 at low angles stray light is usually caused by internal reflections as the angle increase, scattering effect become dominant

,

Chapter 5

Conclusions

5.1 Comments

The main results obtained are twofold. Firstly, for instrument size reduction, diffractive effects compensate for tolerance reductions due to scaling effects. Secondly, the dual groups provide measurable mechanical advantages, given the compensatory effect of optical tolerances and reduced degrees of freedom leading to minimized compounding effects. However, numbers derived from inverse sensitivity are not representative of the real tolerances of the system but are used to assess trends and behaviors. This is because the optical limit imposed is arbitrary, and a more thorough study of astrometric requirements is necessary to establish true optical specifications.

Regarding stray light results, these solely reflect the design work needed for baffles and light traps. The compactness of the design presents challenges in placing these components within the limited space not occupied by the optical path. A study of potential mitigation proposals is thus outlined for future work.

From this thesis, a contributing paper was written for the SPIE Astronomical Telescope + Instrumentation conference[2].

5.2 Future work

The future work can be divided into main aspects: the optical instrument, the development of the prototype and the requirement for a demonstrating mission. Below, we outline the key areas of focus and some ideas for further development:

5.2.1 Further Study of the Optical Instrument System

The presented work aims to analyze the trend of key optomechanical parameters in instrument miniaturization. Subsequently, the work logic for determining the scientific demonstrator is proposed. Firstly, the thermal stability of the instrument needs evaluation, initially as a trend and then with real mission requirements. Thermal requirements derived from the initial analysis can guide mission proposals based on the thermal mitigation capabilities of the selected platform. Radiometric capabilities can then be incorporated into a stray light analysis to assess how changes in the orientation of unwanted light sources affect the S/N ratio across various areas of the focal plane. Following these contextual analyses, identifying scientific applications that could benefit from such observations, despite potentially lower performance, becomes feasible. Performance parameters must also be identified for the demonstrative mission: figures of merit should consider dimensional stability of the system, point spread function characteristics, thermal distributions within the structure, and irradiance on the focal plane. By aligning desired performance, mission capabilities, the preferred platform, mission scope, and demonstrative requirements, and conducting a trade-off among these factors, it is possible to achieve well-defined specifications for a functional and representative prototype.

5.2.2 Prototyping

The construction of the prototype serves to verify the quality of the design against real-world constraints. Primarily, it should demonstrate the advantages and limitations of the RAFTER concept, both from a construction perspective, such as ease of alignment and optical stability in the field, and from a performance perspective, such as constructing a real-case PSF and verifying if the mitigation and stray light requirements are acceptable in practice. Additionally, constructive experience can be gained; manufacturing methods are crucial in defining tolerances and costs. The prototype can then undergo off-design testing to assess the mission envelope and validate the real requirements for remaining subsystems.

5.2.3 Payload Requirements

Drafting the payload requirements is crucial for defining the demonstrative mission. This involves conducting studies to determine the boundary conditions in the operational environment, such as acceptable temperatures, acceptance angles for light sources outside the field of view, and how these aspects affect data acquisition for calibration purposes. Structurally, long-term stability is fundamental within the payload structure, which may need to remain isolated from the rest of the satellite. The attitude determination and control system must ensure the target is within the field of view and maintain this precision throughout the observation duration, aligning with the instrument's resolution (see figure 2.1. Shorter observations can be combined if the control system is not sufficiently stable, generating more data that must interface with a payload computer or an onboard computer for storage and transmission. Data volume is proportional to pixel bit depth (typically 8

to 16 bits) and acquisition resolution:

$$bytes\,of\,data \approx \frac{bit\,depth}{8} \cdot number\,of\,pixel \tag{5.1}$$

The communication system is then sized according to the data volume generated, orbit type, ground station access, and transmission distance. If the data rate or access time is insufficient to transmit all generated data, the onboard computer can perform limited preprocessing, such as isolating relevant stellar PSFs, significantly reducing data volume.

Bibliography

[1] Alberto Riva, Mario Gai, Alberto Vecchiato, Deborah Busonero, Mario Glilberto Lattanzi, Federico Landini, Zhaoxiang Qi, and Zhenghong Tang. Rafter: Ring astrometric field telescope for exo-planets and relativity. In Makenzie Lystrup, Natalie Batalha, Edward C. Tong, Nicholas Siegler, and Marshall D. Perrin, editors, *Space Telescopes and Instrumentation 2020: Optical, Infrared, and Millimeter Wave*. SPIE, December 2020.

[2] F. Stesina M. Gai D. Busonero B. Montrucchio F. Fornasiero, A. Riva and A. Vecchiato. Miniaturization of the rafter optical design for cubesat environment. SPIE, 2024.

[3] D. A. Fischer, A. W. Howard, G. P. Laughlin, B. Macintosh, S. Mahadevan, J. Sahlmann, and J. C. Yee. *Exoplanet Detection Techniques*. University of Arizona Press, 2014.

[4] E Sonbas, N Karaman, A Özdönmez, H Er, K S Dhuga, E Göğüş, I Nasiroglu, and M Zejmo. Probing Transit Timing Variations of three hot Jupiters: HATP-36b, HATP-56b, and WASP-52b. *Monthly Notices of the Royal Astronomical Society*, 509(4):5102–5116, 11 2021.

[5] J. Rameau, G. Chauvin, A. M. Lagrange, A. Boccaletti, S. P. Quanz, M. Bonnefoy, J. H. Girard, P. Delorme, S. Desidera, H. Klahr, C. Mordasini, C. Dumas, M. Bonavita, T. Meshkat, V. Bailey, and M. Kenworthy. Discovery of a probable 4-5 jupiter-mass exoplanet to hd 95086 by direct-imaging, 2013.

[6] Michael Perryman. Hipparcos: a retrospective. 09 2011.

[7] Christoph Cremer and Barry Masters. Resolution enhancement techniques in microscopy. *The European Physical Journal H*, 38, 04 2013.

[8] Busonero, D., Gai, M., Gardiol, D., Lattanzi, M. G., and Loreggia, D. Chromaticity in all-reflective telescopes for astrometry. *AA*, 449(2):827–836, 2006.

[9] C. Fabricius, U. Bastian, J. Portell, J. Castañeda, M. Davidson, N. C. Hambly, M. Clotet, M. Biermann, A. Mora, D. Busonero, A. Riva, A. G. A. Brown, R. Smart, U. Lammers, J. Torra, R. Drimmel, G. Gracia, W. Löffler, A. Spagna, L. Lindegren, S. Klioner, A. Andrei, N. Bach, L. Bramante, T. Brüsemeister, G. Busso, J. M. Carrasco, M. Gai, N. Garralda, J. J. González-Vidal, R. Guerra, M. Hauser, S. Jordan, C. Jordi, H. Lenhardt, F. Mignard, R. Messineo, A. Mulone, I. Serraller, U. Stampa, P. Tanga, A. van Elteren, W. van Reeven, H. Voss, U. Abbas, W. Allasia, M. Altmann, S. Anton, C. Barache, U. Becciani, J. Berthier, L. Bianchi, A. Bombrun, S. Bouquillon, G. Bourda, B. Bucciarelli, A. Butkevich, R. Buzzi, R. Cancelliere, T. Carlucci, P. Charlot, R. Collins, G. Comoretto, N. Cross, M. Crosta, F. de Felice, A. Fienga, F. Figueras, E. Fraile, R. Geyer, J. Hernandez, D. Hobbs, W. Hofmann, S. Liao,

E. Licata, M. Martino, P. J. McMillan, D. Michalik, R. Morbidelli, P. Parsons, M. Pecoraro, M. Ramos-Lerate, M. Sarasso, H. Siddiqui, I. Steele, H. Steidelmüller, F. Taris, A. Vecchiato, A. Abreu, E. Anglada, S. Boudreault, M. Cropper, B. Holl, N. Cheek, C. Crowley, J. M. Fleitas, A. Hutton, J. Osinde, N. Rowell, E. Salguero, E. Utrilla, N. Blagorodnova, M. Soffel, J. Osorio, D. Vicente, J. Cambras, and H.-H. Bernstein. Gaiadata release 1: Pre-processing and source list creation. *Astronomy amp; Astrophysics*, 595:A3, November 2016.

[10] M. Gai, A. Vecchiato, A. Riva, A. G. Butkevich, D. Busonero, Z. Qi, and M. G. Lattanzi. Relative astrometry in an annular field. *Publications of the Astronomical Society of the Pacific*, 134(1033):035001, March 2022.

[11] V. Terebizh. Algorithm for calculating anastigmatic three-mirror telescopes. *Experimental Astronomy*, 49, 04 2020.